Journal of Environmental Chemical Engineering 10 (2022) 108624

Contents lists available at ScienceDirect

Journal of Environmental Chemical Engineering

journal homepage: www.elsevier.com/locate/jece

Optimized removal of antibiotics over $Cd_{0.5}Zn_{0.5}S$/NiCo-LDH : Constructing a homojunctions-heterojunctions composite photocatalyst

Wanyue Dong [a,b], Tao Cai [c,*], Longlu Wang [d], Chuangwei Liu [e], Hui Chen [a,b], Wenlu Li [a,b], Yutang Liu [a,b,**], Xinnian Xia [f]

[a] College of Environmental Science and Engineering, Hunan University, Lushan South Road, Yuelu District, Changsha 410082, PR China
[b] Key Laboratory of Environmental Biology and Pollution Control (Hunan University), Ministry of Education, Lushan South Road, Yuelu District, Changsha 410082, PR China
[c] School of Resource & Environment and Safety Engineering, University of South China, Hengyang 421001, PR China
[d] College of Electronic and Optical Engineering & College of Microelectronics, Nanjing University of Posts and Telecommunications, Nanjing 210023, PR China
[e] Key Lab for Anisotropy and Texture of Materials (MoE), School of Materials Science and Engineering, Northeastern University, Shenyang 110819, PR China
[f] College of Chemistry and Chemical Engineering, Hunan University, Changsha 410082, PR China

ARTICLE INFO

Editor: Dr. G. Palmisano

Keywords:
Photocatalytic degradation
Tetracycline hydrochloride
Norfloxacin
$Cd_{0.5}Zn_{0.5}S$
NiCo-LDH

ABSTRACT

A unique sheet-particle composite structure was constructed via loading NiCo-LDH as a co-catalyst onto the twinning $Cd_{0.5}Zn_{0.5}S$ nanocrystals with inner homojunctions, which benefits to exposing more active sites. The photocatalytic performance of as-prepared catalysts was estimated by the degradation of norfloxacin (NOF) and tetracycline hydrochloride (TC-H) under visible light irradiation. The maximum removal rate of the selected CZS-NiCo8 towards TC-H and NOF over was about 88% and 73%, respectively. Compared with TC-H, the degradation of NOF is more affected by the adsorption of CZS-NiCo8. A series of photoelectric tests demonstrated that the surface type-II heterojunctions were formed between $Cd_{0.5}Zn_{0.5}S$ and NiCo-LDH, due to the enhanced light-harvesting property as well as the optimized photo-generated carrier transit. The radical trapping experiments and ESR results proved that h^+ and $\cdot O_2^-$ were the main active radicals in the degradation of both TC-H and NOF. This work provided some ideas for the design of photocatalysts to remove antibiotics.

1. Introduction

Nowadays, the issue of migration and accumulation of drug residues in the environment has received high attention. As a major portion of medical drug usage, 100,000–200,000 tons of antibiotics are consumed annually [1]. Commonly, antibiotics have a limited biodegradability and fail to be completely eliminated via conventional water treatment technologies, posing potential threats to human health and even the ecological environmental systems [2,3].

Thus, many technologies have been developed to remediate water bodies contaminated by antibiotics. Conventional methods, like membrane filtration, adsorption and biodegradation, are often difficult to meet the demands in terms of cost and efficiency [4,5]. Advanced oxidation technologies, including fenton reaction, electro-catalysis and photo-catalysis, have been widely used for eliminating antibiotics pollutants in recent years[6]. In photocatalytic degradation technologies, the conversion from light energy to chemical energy that can take effect at normal temperatures and pressures is made use of, which is considered to have broad development prospects[7,8].

So far, a diverse range of photocatalysts have been elaborately designed to maximize the conversion and utilization efficiency of solar energy in environmental applications, especially visible-light-driven photocatalysts [3,7]. As a kind of homogeneous solid solution sulfide, $Cd_{1-x}Zn_xS$ was first proposed by Reber's group to improve the catalytic activity of CdS, which also showed advantages including an enhanced stability as well as a tunable band gap in the next few decades [9,10]. However, limited by its intrinsic properties, the photocatalytic activity of pristine $Cd_{1-x}Zn_xS$ is still restricted by the rapid charge recombination[11]. Guo et al. synthesized $Cd_{1-x}Zn_xS$ solid solution with a nano-twin structure, during which the alternating zinc blende/wurtzite (ZB/WZ) homojunctions were induced into a single nanocrystal, and the photocatalytic hydrogen production was dramatically improved

* Corresponding author.
** Corresponding author at: College of Environmental Science and Engineering, Hunan University, Lushan South Road, Yuelu District, Changsha 410082, PR China.
E-mail addresses: ctzz0701@usc.edu.cn (T. Cai), yt_liu@hnu.edu.cn (Y. Liu).

https://doi.org/10.1016/j.jece.2022.108624
Received 8 July 2022; Received in revised form 28 August 2022; Accepted 18 September 2022
Available online 21 September 2022

[11–13]. Besides introducing homojunctions inside the $Cd_{1-x}Zn_xS$, many studies also confirm that by constructing hetero-structures with co-catalysts, kinetics could be boosted for photo-induced carriers [14–16], including metal-free materials, transition metal materials, and noble metal elements. Hence, it is fascinating to integrate hetero-junctions and homojunctions into a two-component composite photo-catalyst [11,15–20].

Layered double hydroxides (LDHs) are a kind of layer-structured semiconductors that are usually composed of two or more different M^{II} and M^{III} metallic cations, which are evenly distributed in the hydroxide layers and octahedrally surrounded by oxo-bridges as well as hydroxyl groups [21,22]. Because the kinds and content of metallic cations are adjustable, LDHs have a flexible light response wavelength range and are extensively studied in the photocatalytic field. According to reports, many LDHs such as ZnCr-LDH[23], CoAl-LDH[24–26], CoZnAl-LDH[27,28], and NiFe-LDH[29–32] etc. are used as co-catalysts in various photocatalytic reactions.

Recently, a few studies on the construction of homojunction-heterojunction-coupled photocatalysts were reported [16,33–35], most of which are twin crystal $Cd_{1-x}Zn_xS$ bases and play a part in photocatalytic hydrogen production. At present, few studies have been done to apply this photocatalyst design concept to the degradation of organic pollutants. Herein, NiCo-LDH was creatively loaded on twinned $Cd_{0.5}Zn_{0.5}S$ nanoparticles to structure a heterojunction-homojunction-coupled composite photocatalyst, which exhibited an enhanced photon-generated carrier separation and transfer ability compared with that of pristine $Cd_{0.5}Zn_{0.5}S$. Meanwhile, through this nanosheet-nanoparticle construction, the morphology and structure of the $Cd_{0.5}Zn_{0.5}S$/NiCo-LDH (CZS-NiCo) composite photocatalyst were optimized. Tetracycline hydrochloride (TC-H) and norfloxacin (NOF) were selected as targeted pollutants to evaluate the photo-degradation capability of CZS-NiCo photocatalysts. The influence of photocatalyst dose, initial concentration, and initial solution pH of TC-H and NOF on the photocatalytic performance of CZS-NiCo8 was discussed, respectively. Free radical capture experiments and ESR technique confirmed that the holes and superoxide radicals were dominant active species during the photo-degradation of both TC-H and NOF, and possible mechanisms of the enhanced photocatalytic degradation activity were then proposed.

2. Experimental section

2.1. Chemicals

All chemicals used in this work were described in Text S1, Supporting Information.

2.2. Synthesis of photocatalysts

2.2.1. Synthesis of twinned $Cd_{0.5}Zn_{0.5}S$ nanocrystal

The twinned $Cd_{0.5}Zn_{0.5}S$ nanocrystals were synthesized through a hydrothermal method according to our previously reported methods (Text S2, Supporting Information) [36–40].

2.2.2. Synthesis of twinned $Cd_{0.5}Zn_{0.5}S$/NiCo-LDH composite catalyst

0.2 g of $Cd_{0.5}Zn_{0.5}S$ was put in 20 mL of H_2O and stirred for 30 min. Meanwhile, 0.5 M mixed solution containing $Co(NO_3)_2 \bullet 6\ H_2O$ and $Ni(NO_3)_2 \bullet 6\ H_2O$ and 1 M NaOH solution were prepared. When $Cd_{0.5}Zn_{0.5}S$ particles were dispersed uniformly, a certain volume of $Ni^{2+} + Co^{2+}$ precursor solution was added dropwise into the mixed solution and continued stirring for 30 min. Then, 1 M NaOH was added slowly to form $NiCo(OH)_2$ on the surface of $Cd_{0.5}Zn_{0.5}S$ particles and keep stirring for 2 h. The volume of 1 M NaOH was 1.5 times than that of $Ni^{2+} + Co^{2+}$ precursor solution. Subsequently, the mixture was transferred to a Teflon-lined stainless-steel autoclave and maintained at 100 °C for 24 h. The as-prepared sample was centrifuged and washed three times with deionized water and ethanol, after which it was dried in an oven at 70 ℃ for 8 h before collecting [21,22]. CZS-NiCo photocatalysts with different LDH loads were prepared, the molar ratio $n_{NiCo\text{-}LDH}$: $n_{Cd0.5Zn0.5S}$= 4%, 8%, and 15%, labeled as CZS-NiCo4, 8, and 15, respectively. The synthesis procedure of CZS-NiCo samples is depicted in Scheme 1.

2.3. Photocatalytic degradation tests

The photocatalytic activity of the samples was evaluated by the degradations of TC-H and NOR under visible light irradiation. A 300 W Xe lamp with a 420 nm cut-off filter was employed as the light source. In each batch of tests, photocatalysts of a certain quality were dispersed in an aqueous solution containing TC-H (50 mL, 50 mg/L) or NOF (50 mL, 5 mg/L). Before light irradiation, the suspension was stirred in the dark for 60 min to gain an adsorption-desorption equilibrium between model compounds and photocatalyst surface. During light irradiation, 1.0 mL of reaction solution was extracted at certain time intervals, which was then percolated through a Millipore-filter with 0.22 μm apertures to remove the residuals. The corresponding concentration of TC-H and NOF was determined via a UV–vis spectrophotometer at their maximum absorption wavelength (356 nm for TC-H and 273 nm for NOF, respectively). The degradation efficiency could be calculated as follows:

$$\text{Removal efficiency}(\%) = \left(1 - \frac{C_t}{C_0}\right) \times 100\%$$

Where C_0 is the initial concentration of TC-H or NOF, and C_t stands for the residual concentration of them during reactions.

Particular characterization methods and detailed parameters of photo-electrochemical examinations are displayed in Text S2 and S3 of Supporting Information.

3. Results and discussion

3.1. Characterization of nanostructured photocatalysts

3.1.1. XRD analysis

Fig. 1 presents the X-ray diffraction (XRD) patterns of the samples obtained. The slight loading of NiCo-LDH didn't obviously affect the XRD pattern of $Cd_{0.5}Zn_{0.5}S$ [41,42], which meant that the nano-twinning characteristic of $Cd_{0.5}Zn_{0.5}S$ was not easily destroyed during this process due to the relatively mild loading conditions. Whereas, in the expanded pattern in Fig. 1a, with an increased loading, two diffraction peaks at 19.2°and 38.2°are observed in CZS-NiCo15[21,22], which could be ascribed to planes (001) and (101) of NiCo-LDH. In addition, the separately synthesized $Cd_{0.5}Zn_{0.5}S$ and NiCo-LDH are also analyzed in Fig. 1b. The diffraction peaks of the obtained NiCo-LDH at 19.1°, 32.9°, 38.2°and 51.8°can be indexed to the (001), (100), (101) and (102) planes of both β-$Co(OH)_2$ (JCPDS No. 30–0443) and β-$Ni(OH)_2$ (JCPDS No. 14–0177), because they are of similar hexagonal structures [43,44]. In the same way, $Cd_{0.5}Zn_{0.5}S$ exhibited a mixed crystal phase of both cubic zinc-blende (ZB) ZnS (JCPDS No. 05–0566) and hexagonal wurtzite (WZ) CdS (JCPDS No. 41–1049), which was due to its solid solution feature, as is mentioned in our previous studies [36,

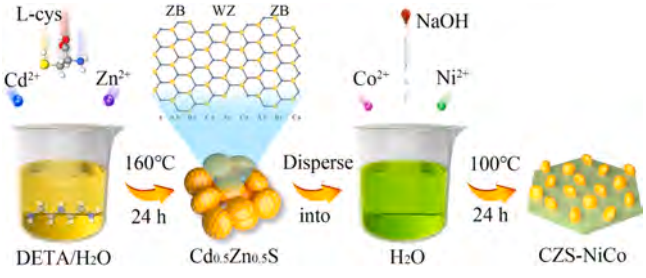

Scheme 1. The synthesis procedure of CZS-NiCo composite samples.

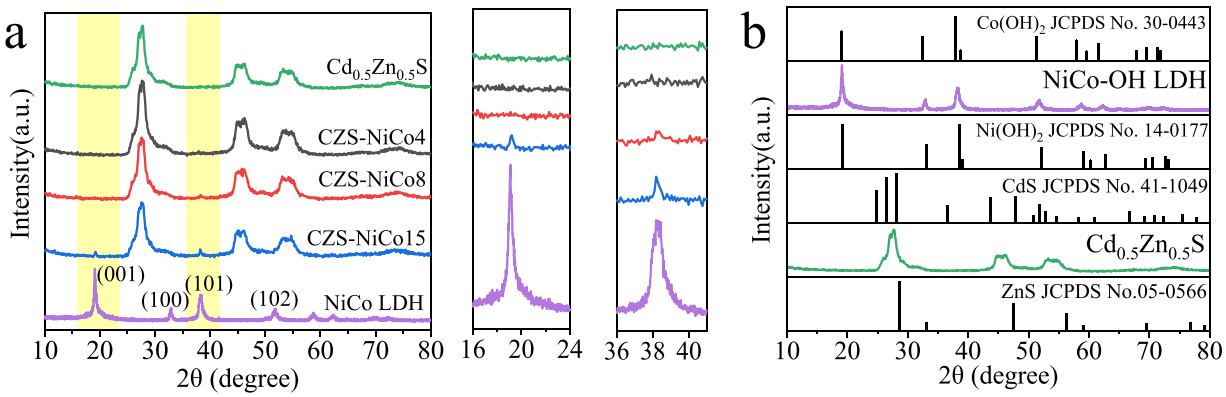

Fig. 1. XRD patterns of as-prepared CZS-NiCo samples (a), pristine $Cd_{0.5}Zn_{0.5}S$ and NiCo-LDH (b).

37].

3.1.2. XPS analysis

The elemental composition, chemical state, and binding energy shift of the as-prepared samples were analyzed via X-ray photoelectron spectroscopy (XPS). The spectra of the overall survey scan of $Cd_{0.5}Zn_{0.5}S$, CZS-NiCo8 and NiCo-LDH are shown in Fig. 2a. Compared to $Cd_{0.5}Zn_{0.5}S$, the signs of Ni and Co element were observed in CZS-NiCo and the intensity of O 1s was increased, indicating the integration of $Cd_{0.5}Zn_{0.5}S$ with NiCo-LDH. As is shown in Fig. 2b and c, the main peaks at 1021.58 and 1044.53 eV were ascribed to Zn $2p_{3/2}$ and Zn $2p_{1/2}$ in $Cd_{0.5}Zn_{0.5}S$[41]; likewise, the XPS peaks appeared at 404.48 eV and 411.23 eV, which were assigned to Cd $3d_{5/2}$ and Cd $3d_{3/2}$. It was identified that both Cd and Zn were of a valence of + 2, and slight shifts towards a higher binding energy were observed in CZS-NiCo8 compared to $Cd_{0.5}Zn_{0.5}S$. In S 2p spectrum (Fig. 2d), the peaks could be divided into two parts corresponding to S $2p_{3/2}$ (161.03 eV) and S $2p_{1/2}$ (162.23 eV), which are characteristic peaks of S^{2-} in $Cd_{0.5}Zn_{0.5}S$ [15], while the binding energy of S $2p_{1/2}$ in CZS-NiCo8 also shifted ($2p_{1/2}$, 163.13 eV), which might be due to the formation of S-metal ions[41].

The Co and Ni spectra of CZS-NiCo8 and NiCo-LDH are shown in Fig. 2e and f, respectively, both of which are composed of two spin-orbit doublets and satellites[45]. In detail, as is shown in Fig. 2e, the peaks at 780.86 and 796.13 eV were assigned to the $2p_{3/2}$ and $2p_{1/2}$ orbit of Co^{3+}, respectively, while those peaks at 783.11 and 798.52 eV were assigned to the $2p_{3/2}$ and $2p_{1/2}$ orbit of Co^{2+}. The analogous feature of mixed-valence state is also exhibited in Ni spectra (Fig. 2f), the peaks at 857.07 and 874.57 eV corresponded to $2p_{3/2}$ and $2p_{1/2}$ orbit of Ni^{3+}, and those peaks at 855.48 and 873.16 eV are attributed to $2p_{3/2}$ and $2p_{1/2}$ orbit of Ni^{2+} The binding energy of both Ni 2p and Co 2p shifted positively than that of pure NiCo-LDH, suggesting that both of them had transferred to higher-valence states [16,46–49]. Considering that all metal species showed negative charges together with S, it could be speculated that electrons tended to transfer from the Ni and Co atoms of NiCo-LDH to S of $Cd_{0.5}Zn_{0.5}S$ [47,49–51]. From the above analysis, the binding energy of all the main elements in the composite was changed, which might be because the interaction between $Cd_{0.5}Zn_{0.5}S$ and NiCo-LDH had simultaneously altered their electron density, confirming that NiCo-LDH had been successfully loaded on the surface of $Cd_{0.5}Zn_{0.5}S$.

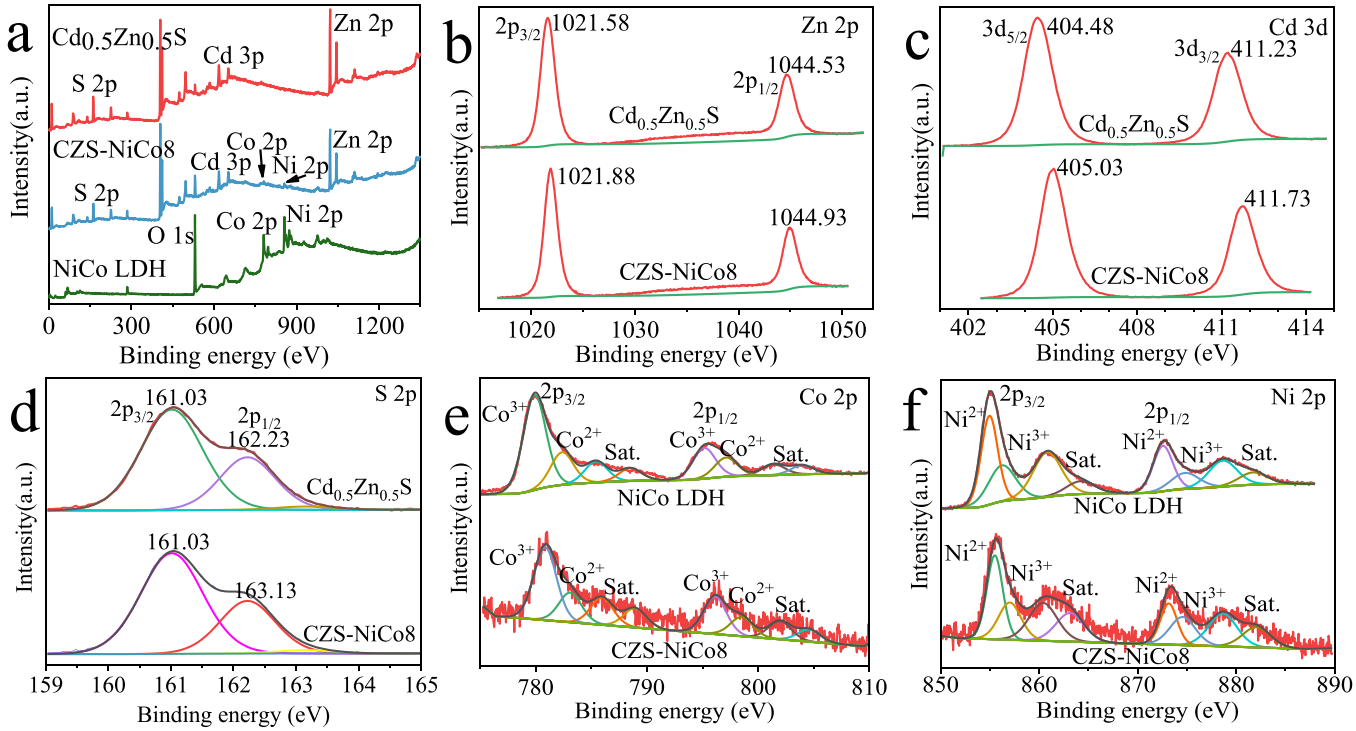

Fig. 2. XPS spectra for survey (a), Zn 2p (b), Cd 3d (c), S 2p (d), Co 2p (e) and Ni 2p (f).

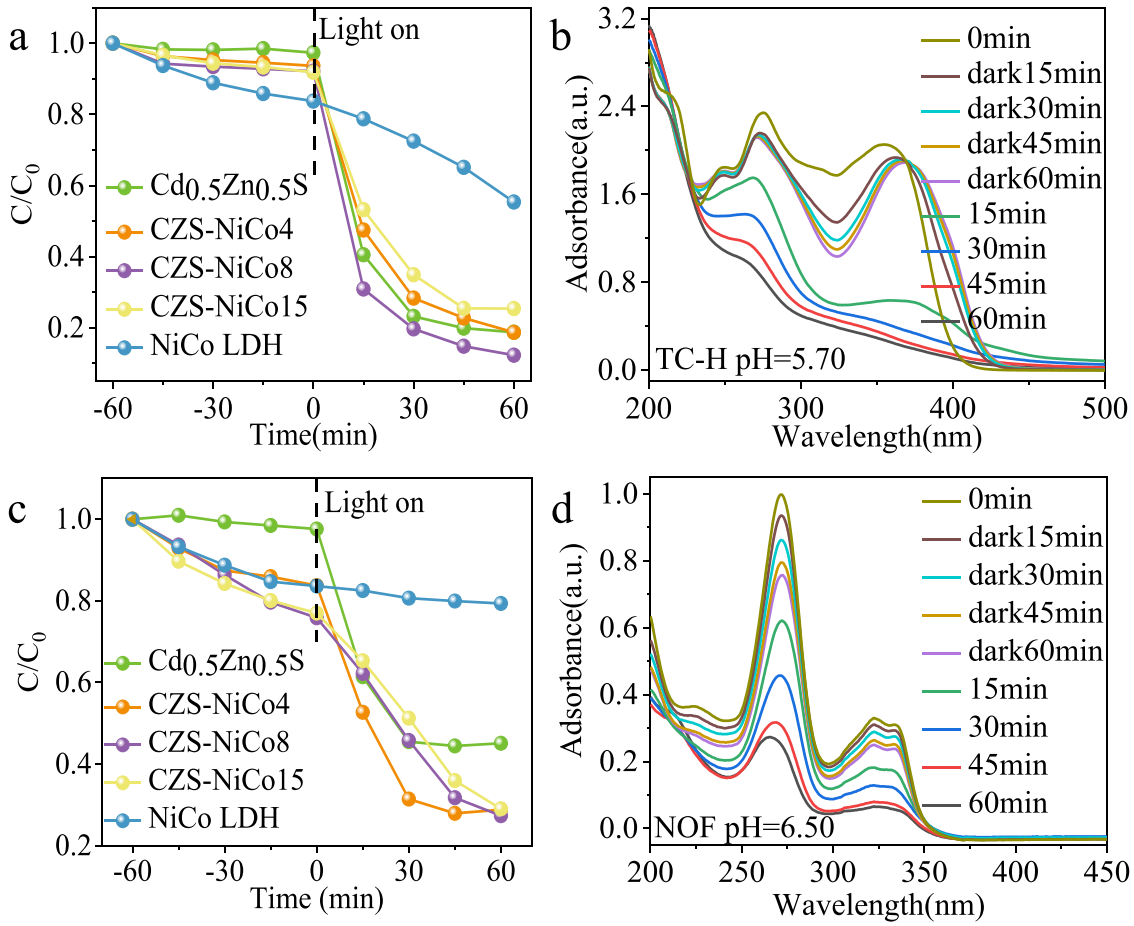

Fig. 5. Photocatalytic degradation of TC-H (a) and NOF (c) by as-prepared samples, and corresponding time-change UV–vis spectra for TC-H (b) and NOF (d) degradation by CZS-NiCo8.

shown in Fig. S4c, with the increasing dose of CZS-NiCo8 catalyst, the NOF removal rate rises from 45.1% to 55.3%, while slightly declines when the catalyst is continuously added. Although more catalysts could theoretically provide more active sites, NOF molecules tend to be adsorbed on the surface of the CZS-NiCo8 catalyst, as is mentioned above, which could hinders the reaction of the catalyst with H_2O to form free radicals, thus the NOF removal efficiency could not be further improved by adding more catalysts. Besides, the existence of catalyst particles also lowered solution transparency and light interception at the same time [69,70].

Similarly, the influence of initial pH on the degradation of NOF is depicted in Fig. S4c, the best removal efficiency of 10 mg/L NOF with 5 mg of CZS-NiCo8 catalyst was obtained at pH = 5, while significantly reduced under extremely acidic (pH = 3) and alkaline (pH = 11) conditions. It could be ascribed to the fact that OH^- ions would compete with anion NOF for active sites on the catalyst surface. As NOF molecules could have three forms at different pH values, namely cation form (pH < 5.46), neutral molecular (5.46 < pH <7.47) and anion form (pH > 7.47) [71], on the premise of considering the stability of catalysts, the electrostatic properties of NOF can be tuned by properly adjusting pH, thus promoting the degradation of NOF through CZS-NiCo8 catalyst.

3.3. Photoelectrical properties

3.3.1. Energy band structures

The optical absorption of as-prepared samples was measured via UV–visible diffuse reflectance spectroscopy (DRS). As is displayed in Fig. 6a, NiCo-LDH presented a wide range (wavelength 200–800 nm) of light absorption, which might be related to its dark green color. Compared with pristine $Cd_{0.5}Zn_{0.5}S$, it was observable that the light absorbance of CZS-NiCo samples was gradually elevated across the wavelength range of 500–800 nm along with NiCo-LDH loading amount [35]. An enhanced light absorption is beneficial for stimulating more photo-induced carriers to carry out redox reactions on the surface of the photocatalysts. Meanwhile, it can be inferred from the almost unchanged absorption edges that NiCo-LDH was loaded on the surface of $Cd_{0.5}Zn_{0.5}S$ rather than doped into crystal lattices. Similarly, it can be seen from the above XRD patterns. The band gap energy of NiCo-LDH and $Cd_{0.5}Zn_{0.5}S$ was calculated via Kubelka–Munk plots (Fig. 6b). The band gap of $Cd_{0.5}Zn_{0.5}S$ and NiCo-LDH was 2.49 eV and 2.10 eV, respectively, which was consistent with previous reports [22,35]. To illustrate the structure of the heterojunctions, a Mott–Schottky (MS) test was used to determine the flat band of $Cd_{0.5}Zn_{0.5}S$ and NiCo-LDH. In Fig. 6c and d, the values obtained are − 0.66 V and − 0.80 V vs. SCE in a 0.5 M Na_2SO_4 solution, corresponding to $Cd_{0.5}Zn_{0.5}S$ and NiCo-LDH, respectively, both of which were determined to be n-type semiconductors due to the positive slopes. Generally, the CB of an n-type semiconductor is 0.1 or 0.2 V more negative than its flat-band potential. Hence, the CB of $Cd_{0.5}Zn_{0.5}S$ and NiCo-LDH can be calculated as − 0.66 V and − 0.80 V vs. NHE according to the formula $E_{NHE} = E_{Ag/AgCl} + 0.1976$. From the above results, both the CB and VB potentials of $Cd_{0.5}Zn_{0.5}S$ was more negative than that of NiCo-LDH, which is in accordance with the band matching mode of type-II heterojunctions.

3.3.2. Charge transfer dynamics

The separation and transfer of the photo-generated carrier was revealed via a series of photochemical measurements. Fig. 7a shows the

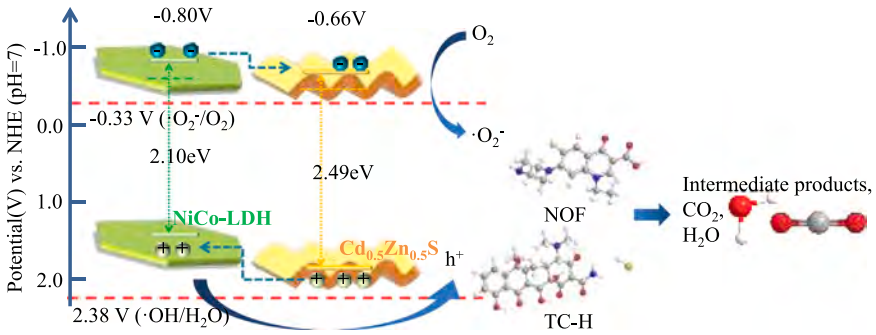

Scheme 2. Photocatalytic mechanism for the degradation of TC-H and NOF pollutants over the CZS-NiCo8 type-II heterojunction system.

mass spectral analysis of the liquid samples taken during the photocatalytic degradation of TC-H with CZS-NiCo8, from which the *m/z* value of the recognizable possible intermediates was labeled and corresponding molecular formulae as well as structures are listed in Table S4[75]. Since the hydroxyl, double bond, and amino groups in TC-H are vulnerable to being attack by reactive radicals, the proposed degradation pathways are shown in Fig. S8. The two main degradation products, TC 1 and TC 2 with the same *m/z* value ($m/z = 461$), are generated through the hydroxylation and carboxylation of TC-H, respectively. TC 3 ($m/z = 459$) is a quinone product generated via the oxidation of $\cdot O_2^-$, and TC 4 ($m/z = 417$) is obtained by breaking the C-N bond in TC-H to lose two methyl groups. When TC 1 was further oxidized, a dehydrogenation reaction occurred, during which TC 5 ($m/z = 459$) was produced [77]; on the other hand, TC 4 underwent deamidation, during which the products TC 6 ($m/z = 357$) and TC 7 ($m/z = 401$) were produced. TC 5–7 again went through a series of ring opening, demethylation, deamination and carbonyl oxidation reactions to obtain smaller molecular structure products TC 8 ($m/z = 283$), TC 9 ($m/z = 242$), TC 10 ($m/z = 147$), etc.

Similarly, some major degradation products were labeled in the mass spectrometric analysis on the liquid samples during the degradation of NOF with CZS-NiCo8 (Fig. S7), and the corresponding molecular formulae and molecular structures are collated in Table S5 [70,78–80]. The inferred degradation pathways of NOF are shown in Fig. S9, the piperazine group in the oxidized NOF is destroyed, obtaining the ring-opening product NOF 1 ($m/z = 350$), and NOF 2 or NOF 3 ($m/z = 322$) was generated due to the loss of a carboxyl group in NOF 1, which was then converted to NOF 4 ($m/z = 242$) through a series of defluorination and quinolone ring destruction processes. Meanwhile, NOF could also first experience defluorination to form NOF 5 ($m/z = 302$). NOF 6 ($m/z = 233$) was yield due to ring-opening and demethylation reactions on NOF 4 and NOF 5, which underwent some deamidation, decarboxylation and ring-opening to form simpler-structural products such as NOF 7 ($m/z = 217$) and NOF 8 ($m/z = 105$). These intermediates will eventually be mineralized to CO_2 and H_2O, as well as other inorganic and harmless substances containing nitrogen and fluorine.

3.5. The reusability of photocatalyst

As another important index to evaluate the practicability of catalysts, the reusability of CZS-NiCo8 was evaluated in four reaction cycles. After each cycle, the catalysts were collected through sedimentation and centrifugation, and fresh TC-H or NOF solution was added for the next cycle. As is shown in Fig. S10a and b, both the removal rate of NOF and TC-H decreases after four times of utilization. Thus, the XRD patterns (Fig. S10c and d) were used to reveal the changes of CZS-NiCo8 before and after reaction. It is observed that the tiny characteristic peaks belonging to NiCo-LDH disappeared when CZS-NiCo8 was used, while the main characteristic peaks were unchanged, implying that the shedding of the co-catalyst NiCo-LDH might occur during the reaction. In Table S1, the element ratio measurement through EDS spectrum shows that the atomic ratio of Ni and Co has declined after the degradation of TC-H and NOF, which is consistent with the XRD pattern results. While, in the EDS mapping images (Fig. S11), it is observed that the overall dispersion density of catalysts increases, indicating that such aggregations could also influence the activity of the catalysts. The element loss condition was investigated with ICP-OES[81], and the element residual concentration of CZS-NiCo8 in TC-H and NOF solutions is depicted in Fig. S12 and Table S6. Therefore, in the next phase of research, we need to pay attention to optimizing preparation methods and improving the reusability of catalysts. Besides, due to the adsorption capacity of CZS-NiCo8 for pollutants, the blockage of the active sites by pollutants and their intermediates is more likely to happen [66].

4. Conclusion

In this study, by fabricating the CZS-NiCo composite photocatalysts, we realized the synergistic effect of homojunctions and heterojunctions, as well as the optimization effect of morphology on catalytic reactions. Except the inner homojunctions possessed by twining $Cd_{0.5}Zn_{0.5}S$ nanocrystals, type-II heterojunctions were formed between $Cd_{0.5}Zn_{0.5}S$ and NiCo-LDH. The loading of NiCo-LDH improved the degradation of both TC-H and NOF, as it not only promoted the separation and transfer of photo-generated carriers, but also enhanced the adsorption capacity of the photocatalysts. TC-H and NOF have different structural and chemical properties, which leads to their different interactions with the catalyst in the degradation reaction. The capturing experiments and ESR tests confirmed that h^+ and $\cdot O_2^-$ were main active radicals in the photodegradation of antibiotic pollutants. This research has revealed the associated photophysical and photochemical processes underlying the above phenomenon, which also provides some reference for the removal of antibiotics.

CRediT authorship contribution statement

Wanyue Dong: Experimental plan formulation and operation, Conceptualization, Methodology, Data processing and analysis, Writing – original draft and modification. **Yutang Liu & Tao Cai:** Formulation and modification of experimental scheme, Conceptualization, Methodology, Writing – review & editing, Data curation. **Chuangwei Liu:** Theoretical calculations. **Hui Chen:** Writing – review & editing, Data curation. **Wenlu Li:** Data curation. **Xinnian Xia:** Writing – review & editing.

Declaration of Competing Interest

The authors declare that they have no known competing financial interests or personal relationships that could have appeared to influence the work reported in this paper.

Data Availability

Data will be made available on request.

Acknowledgements

This work was supported by the National Natural Science Foundation of China (51872089 and 52172087), the Key Laboratory of Jiangxi Province for Persistent Pollutants Control and resources Recycle (Nanchang Hangkong University) (ES201880051). The authors thank National supercomputing center in Changsha for supporting this work.

Appendix A. Supporting information

Supplementary data associated with this article can be found in the online version at doi:10.1016/j.jece.2022.108624.

References

[1] M. Moradi, F. Hasanvandian, A.A. Isari, F. Hayati, B. Setayesh Kakavandi, S.R. Setayesh, CuO and ZnO co-anchored on g-C3N4 nanosheets as an affordable double Z-scheme nanocomposite for photocatalytic decontamination of amoxicillin, 285 (2020) 119838.
[2] H. Mohan, M. Ramasamy, V. Ramalingam, K. Natesan, M. Duraisamy, J. Venkatachalam, T. Shin, K.K. Seralathan, Enhanced visible light-driven photocatalysis of iron-oxide/titania composite: norfloxacin degradation mechanism and toxicity study, J. Hazard Mater. 412 (2021), 125330.
[3] X. Zhang, X. Wang, J. Chai, S. Xue, R. Wang, L. Jiang, J. Wang, Z. Zhang, D. D. Dionysiou, Construction of novel symmetric double Z-scheme $BiFeO_3/CuBi_2O_4/BaTiO_3$ photocatalyst with enhanced solar-light-driven photocatalytic performance for degradation of norfloxacin, Appl. Catal. B Environ. 272 (2020), 119017.
[4] Q. Huang, C. Fang, M. Muhammad, G. Yao, Assessment of norfloxacin degradation induced by plasma-produced ozone using surface-enhanced Raman spectroscopy, Chemosphere 238 (2020), 124618.
[5] Z. Xu, X. Xue, S. Hu, Y. Li, J. Shen, Y. Lan, R. Zhou, F. Yang, C. Cheng, Degradation effect and mechanism of gas-liquid phase dielectric barrier discharge on norfloxacin combined with H_2O_2 or Fe^{2+}, Sep. Purif. Technol. 230 (2020), 115862.
[6] M. Moradi, F. Hasanvandian, A.A. Isari, F. Hayati, B. Kakavandi, S.R. Setayesh, CuO and ZnO co-anchored on g-C_3N_4 nanosheets as an affordable double Z-scheme nanocomposite for photocatalytic decontamination of amoxicillin, Appl. Catal. B Environ. 285 (2021), 119838.
[7] Y. Yang, X. Zhang, C.G. Niu, H.P. Feng, P. Qin, H. Guo, C. Liang, Z. Lei, H. Liu, L. Li, Dual-channel charges transfer strategy with synergistic effect of Z-scheme heterojunction and LSPR effect for enhanced quasi-full-spectrum photocatalytic bacterial inactivation: new insight into interfacial charge transfer and molecular oxygen activation, Appl. Catal. B Environ. 264 (2020), 118465.
[8] C. Sun, L. Wang, W. Zhao, L. Xie, J. Wang, J. Li, B. Li, S. Liu, Z. Zhuang, Q. Zhao, Atomic-level design of active site on two-dimensional MoS_2 toward efficient hydrogen evolution: experiment, Theory, Artif. Intell. Model. (2022) 2206163.
[9] J.F. Reber, M. Rusek, Photochemical hydrogen production with platinized suspensions of cadmium sulfide and cadmium zinc sulfide modified by silver sulfide, J. Phys. Chem. 90 (1986) 824–834.
[10] H. Zhao, H. Liu, R. Sun, Y. Chen, X. Li, A $Zn_{0.5}Cd_{0.5}S$ photocatalyst modified by 2d black phosphorus for efficient hydrogen evolution from water, ChemCatChem 10 (2018) 4395–4405.
[11] Y. Li, B. Sun, H. Lin, Q. Ruan, Y. Geng, J. Liu, H. Wang, Y. Yang, L. Wang, K. Chiu Tam, Efficient visible-light induced H_2 evolution from T-$Cd_xZn_{1-x}S$/defective MoS_2 nano-hybrid with both bulk twinning homojunctions and interfacial heterostructures, Appl. Catal. B Environ. 267 (2020), 118702.
[12] M. Liu, L. Wang, G. Lu, X. Yao, L. Guo, Twins in $Cd_{1-x}Zn_xS$ solid solution: Highly efficient photocatalyst for hydrogen generation from water, Energy Environ. Sci. 4 (2011) 1372–1378.
[13] M. Liu, D. Jing, Z. Zhou, L. Guo, Twin-induced one-dimensional homojunctions yield high quantum efficiency for solar hydrogen generation, Nat. Commun. 4 (2013) 2278.
[14] H.B. Huang, Z.B. Fang, K. Yu, J. Lü, R. Cao, Visible-light-driven photocatalytic H_2 evolution over CdZnS nanocrystal solid solutions: interplay of twin structures, sulfur vacancies and sacrificial agents, J. Mater. Chem. A 8 (2020) 3882–3891.
[15] F.Y. Tian, D. Hou, F. Tang, M. Deng, X.Q. Qiao, Q. Zhang, T. Wu, D.S. Li, Novel $Zn_{0.8}Cd_{0.2}S$@g-C_3N_4 core-shell heterojunctions with a twin structure for enhanced visible-light-driven photocatalytic hydrogen generation, J. Mater. Chem. A 6 (2018) 17086–17094.
[16] C. Wang, X. Ma, Z. Fu, X. Hu, J. Fan, E. Liu, Highly efficient photocatalytic H_2 evolution over $NiCo_2S_4/Mn_{0.5}Cd_{0.5}S$: Bulk twinned homojunctions and interfacial heterojunctions, J. Colloid Interface Sci. 592 (2021) 66–76.
[17] Y. Chew, B. Ng, X.Y. Kong, L.K. Putri, J. Tang, L. Tan, S.P. Chai, Fuels, Interfacial engineering of a zinc blende/wurtzite homojunction photocatalyst through hybridization with a cobalt phosphide co-catalyst for enhanced visible-light-driven photocatalytic H2 evolution,4 (2020) 1822–1827.
[18] C. Xue, X. Yan, H. An, H. Li, J. Wei, G. Yang, Bonding CdS-Sn_2S_3 eutectic clusters on graphene nanosheets with unusually photoreaction-driven structural reconfiguration effect for excellent H_2 evolution and Cr(VI) reduction, Appl. Catal. B Environ. 222 (2018) 157–166.
[19] J. Song, H. Zhao, R. Sun, X. Li, D. Sun, An efficient hydrogen evolution catalyst composed of palladium phosphorous sulphide ($PdP_{-0.33}S_{-1.67}$) and twin nanocrystal $Zn_{0.5}Cd_{0.5}S$ solid solution with both homo- and hetero-junctions, Energy Environ. Sci. 10 (2017) 225–235.
[20] M. Liu, Y. Chen, J. Su, J. Shi, X. Wang, L. Guo, Photocatalytic hydrogen production using twinned nanocrystals and an unanchored NiS_x co-catalyst, Nat. Energy 1 (2016) 1–8.
[21] F. Meng, Y. Qin, J. Lu, X. Lin, M. Meng, G. Sun, Y. Yan, Biomimetic design and synthesis of visible-light-driven g-C_3N_4 nanotube @polydopamine/NiCo-layered double hydroxides composite photocatalysts for improved photocatalytic hydrogen evolution activity, J. Colloid Interface Sci. 584 (2021) 464–473.
[22] S. Li, L. Wang, Y. Li, L. Zhang, A. Wang, N. Xiao, Y. Gao, N. Li, W. Song, L. Ge, J. Liu, Novel photocatalyst incorporating Ni-Co layered double hydroxides with P-doped CdS for enhancing photocatalytic activity towards hydrogen evolution, Appl. Catal. B Environ. 254 (2019) 145–155.
[23] B. Luo, R. Song, D. Jing, ZnCr LDH nanosheets modified graphitic carbon nitride for enhanced photocatalytic hydrogen production, Int. J. Hydrogen Energ. 42 (2017) 23427–23436.
[24] P. Cai, S. Ci, N. Wu, Y. Hong, Z. Wen, Layered structured CoAl/CdS-LDHs nanocomposites as visible light photocatalyst, Phys. Status Solidi a 214 (2017) 1600910.
[25] W. He, R. Wang, L. Zhang, J. Zhu, X. Xiang, F. Li, Enhanced photoelectrochemical water oxidation on a $BiVO_4$ photoanode modified with multi-functional layered double hydroxide nanowalls, J. Mater. Chem. A 3 (2015) 17977–17982.
[26] W.K. Jo, S. Tonda, Novel CoAl-LDH/g-C_3N_4/RGO ternary heterojunction with notable 2D/2D/2D configuration for highly efficient visible-light-induced photocatalytic elimination of dye and antibiotic pollutants, J. Hazard Mater. 368 (2019) 778–787.
[27] Y. Yang, J. Wu, T. Xiao, Z. Tang, J. Shen, H. Li, Y. Zhou, Z. Zou, Urchin-like hierarchical CoZnAl-LDH/RGO/g-C_3N_4 hybrid as a Z-scheme photocatalyst for efficient and selective CO_2 reduction, Appl. Catal. B Environ. 255 (2019), 117771.
[28] A.R. Amani-Ghadim, F. Khodam, M.S. Seyed, Dorraji, ZnS quantum dot intercalated layered double hydroxide semiconductors for solar water splitting and organic pollutant degradation, J. Mater. Chem. A 7 (2019) 11408–11422.
[29] A. Khataee, T. Sadeghi Rad, S. Nikzat, A. Hassani, M.H. Aslan, M. Kobya, E. Demirbaş, Fabrication of NiFe layered double hydroxide/reduced graphene oxide (NiFe-LDH/rGO) nanocomposite with enhanced sonophotocatalytic activity for the degradation of moxifloxacin, Chem. Eng. J. 375 (2019), 122102.
[30] S. Nayak, G. Swain, K. Parida, Enhanced photocatalytic activities of RhB degradation and H_2 evolution from in situ formation of the electrostatic heterostructure MoS_2/NiFe LDH nanocomposite through the Z-scheme mechanism via p-n heterojunctions, ACS Appl. Mater. Interfaces 11 (2019) 20923–20942.
[31] J. Zhang, L. Yu, Y. Chen, X.F. Lu, S. Gao, X.W. Lou, Designed formation of double-shelled Ni-Fe layered-double-hydroxide nanocages for efficient oxygen evolution reaction, Adv. Mater. 32 (2020), e1906432.
[32] Y. Wu, Y. Gong, J. Liu, T. Chen, Q. Liu, Y. Zhu, L. Niu, C. Li, X. Liu, C.Q. Sun, S. Xu, Constructing NiFe-LDH wrapped Cu_2O nanocube heterostructure photocatalysts for enhanced photocatalytic dye degradation and CO_2 reduction via Z-scheme mechanism, J. Alloy. Compd. 831 (2020).
[33] L. Guo, G. Yu, H. Zhao, C. Xing, Y. Hu, T. Chen, X. Li, Construction of heterojunctions between ReS_2 and twin crystal $Zn_xCd_{1-x}S$ for boosting solar hydrogen evolution, New J. Chem. 45 (2021) 5137–5145.
[34] P. Mu, M. Zhou, K. Yang, X. Chen, Z. Yu, K. Lu, W. Huang, C. Yu, W. Dai, $Cd_{0.5}Zn_{0.5}S/CoWO_4$ nanohybrids with a twinning homojunction and an interfacial S-scheme heterojunction for efficient visible-light-induced photocatalytic CO_2 reduction, Inorg. Chem. 60 (2021) 14854–14865.
[35] Y.H. Chew, B.J. Ng, X.Y. Kong, L.K. Putri, J.Y. Tang, L.L. Tan, S.P. Chai, Interfacial engineering of a zinc blende/wurtzite homojunction photocatalyst through hybridization with a cobalt phosphide co-catalyst for enhanced visible-light-driven photocatalytic H_2 evolution, Sustain. Energy Fuels 4 (2020) 1822–1827.
[36] W. Dong, Y. Liu, G. Zeng, T. Cai, L. Shao, H. Chen, W. Zeng, X. Xia, Crystal phase engineering $Zn_{0.8}Cd_{0.2}S$ nanocrystals with twin-induced homojunctions for photocatalytic nitrogen fixation under visible light, J. Photochem. Photobiol. A Chem. 401 (2020), 112766.
[37] W. Dong, Y. Liu, G. Zeng, S. Zhang, T. Cai, J. Yuan, H. Chen, J. Gao, C. Liu, Regionalized and vectorial charges transferring of $Cd_{1-x}Zn_xS$ twin nanocrystal homojunctions for visible-light driven photocatalytic applications, J. Colloid Interface Sci. 518 (2018) 156–164.
[38] H. Du, K. Liang, C.Z. Yuan, H.L. Guo, X. Zhou, Y.F. Jiang, A.W. Xu, Bare $Cd_{1-x}Zn_xS$ ZB/WZ Heterophase Nanojunctions for Visible Light Photocatalytic Hydrogen Production with High Efficiency, ACS Appl. Mater. Interfaces 8 (2016) 24550–24558.
[39] M. Liu, B. Wang, Y. Zheng, F. Xue, Y. Chen, L. Guo, Transformation of zincblende nanoparticles into wurtzite microrods by a dissolution–regrowth process: an intergrowth homojunction with enhanced photocatalytic activity, Catal. Sci. Technol. 6 (2016) 3371–3377.
[40] M. Liu, L. Zhang, X. He, B. Zhang, H. Song, S. Li, W. You, l-Cystine-assisted hydrothermal synthesis of $Mn_{1-x}Cd_xS$ solid solutions with hexagonal wurtzite structure for efficient photocatalytic hydrogen evolution under visible light irradiation, J. Mater. Chem. A 2 (2014) 4619–4626.
[41] X. Li, R. He, Y. Dai, S. Li, N. Xiao, A. Wang, Y. Gao, N. Li, J. Gao, L. Zhang, L. Ge, Design and fabrication of $Co_9S_8/Zn_{0.5}Cd_{0.5}S$ hollow nanocages with significantly

enhanced photocatalytic hydrogen production activity, Chem. Eng. J. 400 (2020), 125474.
[42] D. Dai, L. Wang, N. Xiao, S. Li, H. Xu, S. Liu, B. Xu, D. Lv, Y. Gao, W. Song, L. Ge, J. Liu, In-situ synthesis of Ni_2P co-catalyst decorated $Zn_{0.5}Cd_{0.5}S$ nanorods for high-quantum-yield photocatalytic hydrogen production under visible light irradiation, Appl. Catal. B Environ. 233 (2018) 194–201.
[43] H. Gao, G. Wang, M. Yang, L. Tan, J. Yu, Novel tunable hierarchical Ni–Co hydroxide and oxide assembled from two-wheeled units, Nanotechnology 23 (2012).
[44] X. Li, H. Wu, A.M. Elshahawy, L. Wang, S.J. Pennycook, C. Guan, J. Wang, Cactus-Like NiCoP/NiCo-OH 3D architecture with tunable composition for high-performance electrochemical capacitors, Adv. Funct. Mater. 28 (2018).
[45] X. Li, H. Wu, C. Guan, A.M. Elshahawy, Y. Dong, S.J. Pennycook, J. Wang, Ni,Co) Se_2/NiCo-LDH core/shell structural electrode with the cactus-like (Ni,Co)Se_2 core for asymmetric supercapacitors, Small 15 (2019) 1803895.
[46] W. Chang, W. Xue, E. Liu, J. Fan, B. Zhao, Highly efficient H_2 production over $NiCo_2O_4$ decorated g-C_3N_4 by photocatalytic water reduction, Chem. Eng. J. 362 (2019) 392–401.
[47] Q. Cao, S. Hao, Y. Wu, K. Pei, W. You, R. Che, Interfacial charge redistribution in interconnected network of Ni_2P-Co_2P boosting electrocatalytic hydrogen evolution in both acidic and alkaline conditions, Chem. Eng. J. 424 (2021), 130444.
[48] J. Yu, J. Wang, X. Long, L. Chen, Q. Cao, J. Wang, C. Qiu, J. Lim, S. Yang, Formation of FeOOH nanosheets induces substitutional doping of CeO_{2-x} with high-valence Ni for efficient water oxidation, Adv. Energy Mater. 11 (2020) 2002731.
[49] Y. Lin, K. Sun, X. Chen, C. Chen, Y. Pan, X. Li, J. Zhang, High-precision regulation synthesis of Fe-doped Co_2P nanorod bundles as efficient electrocatalysts for hydrogen evolution in all-pH range and seawater, J. Energy Chem. 55 (2021) 92–101.
[50] W. Nie, Q. Mao, Y. Ding, Y. Hu, H. Tang, Highly efficient catalysis of chalcopyrite with surface bonded ferrous species for activation of peroxymonosulfate toward degradation of bisphenol A: a mechanism study, J. Hazard. Mater. 364 (2019) 59–68.
[51] J. Peng, X. Lu, X. Jiang, Y. Zhang, Q. Chen, B. Lai, G. Yao, Degradation of atrazine by persulfate activation with copper sulfide (CuS): kinetics study, degradation pathways and mechanism, Chem. Eng. J. 354 (2018) 740–752.
[52] B.J. Ng, L.K. Putri, X.Y. Kong, P. Pasbakhsh, S.P. Chai, Overall pure water splitting using one-dimensional P-doped twinned $Zn_{0.5}Cd_{0.5}S_{1-x}$ nanorods via synergetic combination of long-range ordered homojunctions and interstitial S vacancies with prolonged carrier lifetime, Appl. Catal. B Environ. 262 (2020), 118309.
[53] K. Yuan, Q. Cao, H.L. Lu, M. Zhong, X. Zheng, H.Y. Chen, T. Wang, J.J. Delaunay, W. Luo, L. Zhang, Y.Y. Wang, Y. Deng, S.J. Ding, D.W. Zhang, Oxygen-deficient WO_{3-x}@TiO_{2-x} core-shell nanosheets for efficient photoelectrochemical oxidation of neutral water solutions, J. Mater. Chem. A 5 (2017) 14697–14706.
[54] H. She, P. Yue, X. Ma, J. Huang, L. Wang, Q. Wang, Fabrication of $BiVO_4$ photoanode cocatalyzed with NiCo-layered double hydroxide for enhanced photoactivity of water oxidation, Appl. Catal. B Environ. 263 (2020), 118280.
[55] J. Wang, F. Gao, X. Du, X. Ma, X. Hao, W. Ma, K. Wang, G. Guan, A. Abudula, A high-performance electroactive PPy/rGO/NiCo-LDH hybrid film for removal of dilute dodecyl sulfonate ions, Electrochim. Acta 331 (2020).
[56] Z. Zhao, H. Wu, H. He, X. Xu, Y. Jin, A High-Performance Binary Ni–Co Hydroxide-based Water Oxidation Electrode with Three-Dimensional Coaxial Nanotube Array Structure, Adv. Funct. Mater. 24 (2014) 4698–4705.
[57] Y.Y. Hsu, N.T. Suen, C.C. Chang, S.F. Hung, C.L. Chen, T.S. Chan, C.L. Dong, C. C. Chan, S.Y. Chen, H.M. Chen, Heterojunction of zinc Blende/Wurtzite in $Zn_{1-x}Cd_xS$ solid solution for efficient solar hydrogen generation: X-ray absorption/diffraction approaches, ACS Appl. Mater. Interfaces 7 (2015) 22558–22569.
[58] P. Caroff, K.A. Dick, J. Johansson, M.E. Messing, K. Deppert, L. Samuelson, Controlled polytypic and twin-plane superlattices in iii-v nanowires, Nat. Nanotechnol. 4 (2009) 50–55.
[59] Q. Cao, R. Che, N. Chen, Scalable synthesis of Cu_2S double-superlattice nanoparticle systems with enhanced UV/visible-light-driven photocatalytic activity, Appl. Catal. B Environ. 162 (2015) 187–195.
[60] Q. Cao, Y.F. Cheng, H. Bi, X. Zhao, K. Yuan, Q. Liu, Q. Li, M. Wang, R. Che, Crystal defect-mediated band-gap engineering: a new strategy for tuning the optical properties of Ag_2Se quantum dots toward enhanced hydrogen evolution performance, J. Mater. Chem. A 3 (2015) 20051–20055.
[61] Y. Sun, C. Xu, H. Ma, G. Li, L. Chen, Y. Sun, Z. Chen, P. Fang, Q. Fu, C. Pan, Synthesis of flower-liked twin crystal ternary Ni/NiS/Zn0.2Cd0.8S catalyst for highly efficient hydrogen production, Chem. Eng. J. 406 (2021), 126878.
[62] K. Liu, H. Zhang, Y. Muhammad, T. Fu, R. Tang, Z. Tong, Y. Wang, Fabrication of n-n isotype BiOBr-Bi_2WO_6 heterojunctions by inserting Bi_2WO_6 nanosheets onto BiOBr microsphere for the superior photocatalytic degradation of Ciprofloxacin and tetracycline, Sep. Purif. Technol. 274 (2021), 118992.
[63] Z. Jian, C. Shao, X. Li, J. Xin, T. Ran, Y. Liu, Engineering, assembling n-Bi_2MoO_6 nanosheets on electrospun p-$CuAl_2O_4$ hollow nanofibers: enhanced photocatalytic activity based on highly efficient charge separation and transfer, ACS Sustain. Chem. Eng. 6 (2018) 10714–10723.
[64] D. Zhang, J. Li, Q. Wang, High {001} facets dominated BiOBr lamellas: facile hydrolysis preparation and selective visible-light photocatalytic activity, J. Mater. Chem. A 1 (30) (2013) 8622–8629.
[65] Y. Luo, J. Chen, C. Wu, J. Zhang, J. Tang, J. Shang, Q. Liao, Effect of particle size on adsorption of norfloxacin and tetracycline onto suspended particulate matter in lake, Environ. Pollut. 244 (2019) 549–559.
[66] X. Lv, D.Y.S. Yan, F.L.Y. Lam, Y.H. Ng, S. Yin, A.K. An, Solvothermal synthesis of copper-doped BiOBr microflowers with enhanced adsorption and visible-light driven photocatalytic degradation of norfloxacin, Chem. Eng. J. 401 (2020), 126012.
[67] X. Lian, W. Xue, S. Dong, E. Liu, H. Li, K. Xu, Construction of S-scheme Bi_2WO_6/g-C_3N_4 heterostructure nanosheets with enhanced visible-light photocatalytic degradation for ammonium dinitramide, J. Hazard Mater. 412 (2021), 125217.
[68] M. Murugalakshmi, G. Mamba, S.A. Ansari, V. Muthuraj, T.I.T. Nkambule, Ultrasonic assisted anchoring of Yb_2O_3 nanorods on In_2S_3 nanoflowers for norfloxacin degradation and Cr(VI) reduction in water: kinetics and degradation pathway, Coll. Surf. A Physicochem. Eng. Asp. 634 (2022), 127969.
[69] C. Chen, R. Bao, L. Yang, S. Tai, Y. Zhao, W. Wang, J. Xia, H. Li, Application of inorganic perovskite $LaNiO_3$ partial substituted by Ce and Cu in absorbance and photocatalytic degradation of antibiotics, Appl. Surf. Sci. 579 (2022).
[70] C. Zhang, M. Jia, Z. Xu, W. Xiong, Z. Yang, J. Cao, H. Peng, H. Xu, Y. Xiang, Y. Jing, Constructing 2D/2D N-ZnO/g-C_3N_4 S-scheme heterojunction: efficient photocatalytic performance for norfloxacin degradation, Chem. Eng. J. 430 (2022), 132652.
[71] N. Yin, H. Chen, X. Yuan, Y. Zhang, M. Zhang, J. Guo, Y. Zhang, L. Qiao, M. Liu, K. Song, Highly efficient photocatalytic degradation of norfloxacin via $Bi_2Sn_2O_7$/PDIH Z-scheme heterojunction: Influence and mechanism, J. Hazard Mater. 436 (2022), 129317.
[72] Q. Ruan, X. Ma, Y. Li, J. Wu, Z. Wang, Y. Geng, W. Wang, H. Lin, L. Wang, One-dimensional CdS@$Cd_{0.5}Zn_{0.5}S$@ZnS-Ni$(OH)_2$ nano-hybrids with epitaxial heterointerfaces and spatially separated photo-redox sites enabling highly-efficient visible-light-driven H_2 evolution, Nanoscale 12 (2020) 20522–20535.
[73] F. Yi, H. Gan, H. Jin, W. Zhao, K. Zhang, H. Jin, H. Zhang, Y. Qian, J. Ma, Sulfur- and chlorine-co-doped g-C_3N_4 nanosheets with enhanced active species generation for boosting visible-light photodegradation activity, Sep. Purif. Technol. 233 (2020).
[74] X. Ding, K. Zhao, L. Zhang, Enhanced photocatalytic removal of sodium pentachlorophenate with self-doped Bi_2WO_6 under visible light by generating more superoxide ions, Environ. Sci. Technol. 48 (2014) 5823.
[75] B. Lin, S. Li, Y. Peng, Z. Chen, X. Wang, MOF-derived core/shell C-TiO_2/$CoTiO_3$ type II heterojunction for efficient photocatalytic removal of antibiotics, J. Hazard. Mater. 406 (2021), 124675.
[76] J. Tang, J. Wang, L. Tang, C. Feng, X. Zhu, Y. Yi, H. Feng, J. Yu, X. Ren, Preparation of floating porous g-C_3N_4 photocatalyst via a facile one-pot method for efficient photocatalytic elimination of tetracycline under visible light irradiation, Chem. Eng. J. 430 (2021), 132669.
[77] R. Tang, D. Gong, Y. Deng, S. Xiong, J. Zheng, L. Li, Z. Zhou, L. Su, J. Zhao, π-π stacking derived from graphene-like biochar/g-C_3N_4 with tunable band structure for photocatalytic antibiotics degradation via peroxymonosulfate activation, J. Hazard Mater. 423 (2021), 126944.
[78] X.J. Wen, C.G. Niu, D.W. Huang, L. Zhang, C. Liang, G.M. Zeng, Study of the photocatalytic degradation pathway of norfloxacin and mineralization activity using a novel ternary Ag/AgCl-CeO_2 photocatalyst, J. Catal. 355 (2017) 73–86.
[79] J. Guo, C.H. Shen, J. Sun, X.J. Xu, X.Y. Li, Z.H. Fei, Z.T. Liu, X.J. Wen, Highly efficient activation of peroxymonosulfate by Co_3O_4/Bi_2MoO_6 p-n heterostructure composites for the degradation of norfloxacin under visible light irradiation, Sep. Purif. Technol. 259 (2021), 118109.
[80] C. Feng, Y. Wang, Z. Lu, Q. Liang, Y. Zhang, Z. Li, S. Xu, Nanoflower Ni_5P_4 coupled with GCNQDs as Schottky junction photocatalyst for the efficient degradation of norfloxacin, Sep. Purif. Technol. 282 (2022), 120107.
[81] X. Xu, Y. Yang, J. Han, P. Bing, C. Jiang, D. Shao, J. Shi, Filamentous fungal in situ biosynthesis of heterogeneous Au/Cd0.5Zn0.5S nano-photocatalyst: A macroscopic assembly strategy for preparing composite mycelial pellets with visible light degradation ability, 406 (2020) 124797.